

Characterization of Trace and Rare Earth Element in the gneissic rocks from the Bundelkhand Craton, Central India

Pratigya Pathak ^{#1}, Shyam Bihari Dwivedi ^{*2}

Department of Civil Engineering, Indian Institute of Technology (BHU), Varanasi-221005, India

pratigyapathak.rs.civ17@itbhu.ac.in

sbd.civ@iitbhu.ac.in

Article Info

Page Number: 24 - 36

Publication Issue:

Vol 71 No. 4 (2022)

Abstract

The geochemical compositions of gneissic rock samples from the Bundelkhand Craton were studied in order to determine their provenance, the nature of original sediments, and their tectonic setting. These rocks have an abundance of Rb, Ba, La, Ce, and Gd and depletion of Mo, Ho, Tm, Nb, Ta, Sr, Hf, and Ti. A negative anomaly of Nb and Ti suggests a subduction-related environment. The discrimination diagram of $\log(\text{Fe}_2\text{O}_3/\text{K}_2\text{O})$ vs $\log(\text{SiO}_2/\text{Al}_2\text{O}_3)$ shows that the parental rock of the gneissic rocks is shale. The $\text{P}_2\text{O}_5/\text{TiO}_2$ vs MgO/CaO plot indicates the recycled sedimentary origin of the rocks. The SiO_2 vs $\log(\text{Na}_2\text{O}/\text{K}_2\text{O})$ diagram suggests that the gneissic rocks were deposited in the active continental margin setting. According to tectonic discrimination diagrams with a discrimination function and a binary plot of TiO_2 against Zr, the gneissic rocks were derived from felsic igneous rocks. The trace element plots $(\text{Th}/\text{Nb})_N$ vs $(\text{Y}/\text{Nb})_N$ and Nb/Zr vs Zr show that gneissic rocks were deposited in an active convergent margin from a felsic igneous source, then transported and metamorphosed.

Article History

Article Received: 25 March 2022

Revised: 30 April 2022

Accepted: 15 June 2022

Publication: 19 August 2022

Keywords: Geochemistry, Provenance, Tectonic Setting, Metamorphism, Bundelkhand Craton

Introduction

Sediments are derived from rocks, soil, or biological material and then transported and deposited as particles or aggregates. As a general rule, all sediments are weathering products of basement rocks. Various mining and environmental studies use sediment chemistry to identify minerals and trace elements [1]. Geochemical investigations based on rock chemical analysis are a helpful instrument with many uses. Based on quantitative measurement and patterns of geochemical variations, geochemistry is the most effective tool to discriminate between igneous rock suits, identify involved magmatic processes, the nature of melt and protolith, and determine the tectonothermal environment. Geochemistry is a broad term for the science that deals with all geological studies that involve chemical change. It entails the investigation of element distributions in minerals, rocks, soils, and various earth materials. Our comprehension of many geological processes is based on visualizing major, minor, and trace elements in a rock. Rapid characterization of geochemical zoning in larger samples adds context to subsequent inquiry, permitting more robust

sub-sampling decisions for other analytical procedures and decreasing the total number of samples analyzed by more expensive techniques.

The most abundant oxides in rocks, which deal with the order of increasing atomic numbers, are the oxides of sodium (Na_2O), magnesium (MgO), aluminium (Al_2O_3), silicon (SiO_2), phosphorus (P_2O_5), potassium (K_2O), calcium (CaO), titanium (TiO_2), manganese (MnO) and iron (both ferric Fe_2O_3 and ferrous FeO). They are mostly used for rock classification and the construction of variation diagrams. Major elements are present in an amount on the Earth's crust of more than 1wt %, and trace elements are less than 1 wt %. The behaviour of the major oxides in magmas can be manifested in terms of the differentiation index. Likewise, trace elements behave similarly to major oxides because they substitute for some elements in major oxides. The term "rare earth elements" (REEs) does not imply that they are uncommon in nature; rather, REEs are quite common. In the average crust, the total amount of REEs exceeds 200 ppm. Some REEs are even more prevalent in the crust than copper or lead [2-3]. REEs are a group of 15 (trace) elements with atomic numbers ranging from 57 (La) to 71 (Lu); 14 of these elements occur naturally (except Promethium-Pm). For convenience, the REEs are divided into two sub-groups: (i) The light rare earth elements (LREE) range from La to Sm, while the heavy rare earth elements (HREE) range from Gd to Lu. However, middle rare earth elements (MREE) are elements from about Sm to Ho [4]. In nature, all of the rare earth elements exhibit a 3+ oxidation state (trivalent), except Ce^{4+} (oxidized) and Eu^{2+} (reduced) under most geological conditions. REEs are normally deemed immobile after igneous alteration and low-grade metamorphism. REE patterns help understand the petrogenesis process and the tectonic discrimination setting of different rocks. It is fascinating to decide whether the metamorphic rocks' protolith is of sedimentary or igneous origin, with many discrimination diagrams employed in the literature.

Most of the Bundelkhand Craton (BuC) consists of rocks with important mineral constituents. These are mainly igneous and metamorphic rocks. Till now, the geochemistry of the fine-grained rocks of the BuC has not been well investigated in order to understand its source rock properties, provenance, and tectonic setting. Using major, trace, and rare earth element (REEs) geochemistry, this study attempted to evaluate the geochemistry of the study area's gneissic rocks to offer information on source rock properties, provenances, and tectonic context.

Study area

Among the many Archean cratons of India, the Bundelkhand craton (BuC) has the most complex evolutionary history [5]. It is semicircular to triangular and has an area of about 45,000 km^2 , of which only 26,000 km^2 is exposed as an outcrop, and the rest is covered by the alluvium of the Ganga basin [6]. The east-west trending Son–Narmada lineament (SONA) bounds BuC in the south, the NE-SW trending Great Boundary Fault (GBF) in the west, and the WNW–ESE trending Yamuna fault in the north [7-8] (Fig.1).

BuC is mainly characterized by Bundelkhand Granite, tonalite trondjemite granodiorite (TTG) gneisses, dyke swarms of mafic composition trending NW–SE, NE–SW trending quartz reefs, and high-grade supracrustals and metavolcanic. Supracrustal rocks of pelitic composition have also been delineated in the BuC [9]. Based on new geological and geophysical data, two tectonic divisions are established: the Central Bundelkhand terrain and the Southern Bundelkhand

terrain [7]. The central Bundelkhand terrain consists mainly of the Babina-Mauranipur-Mahoba belt. This belt comprises a granite-greenstone complex striking in an E–W direction. This granite-greenstone complex embraces TTG of the Paleo-Neoproterozoic age, greenstone rocks of the Meso-Neoproterozoic age, a granodiorite-granite suite of the Neoproterozoic age, and oceanic rocks of the Paleoproterozoic age. Despite these rocks, lavas of mafic to ultramafic composition, volcanic of felsic composition (lava and dykes), and metasedimentary rocks (BIFs) are also present [10]. The Central and Southern Bundelkhand terrains display a singular crustal architecture, evolution, geological structure, and Sm-Nd model age of granitoid. The four main stages that indulge in continental crust formation for BuC were described [11], which are (1) 3.55–3.2 Ga-granitoids (tonalite–trondhjemite–granodiorite association), the oldest. (2) 2.82–2.8 Ga Central-Bundelkhand greenstone complex is composed of felsic volcanic from the Mauranipur greenstone belt. (3) 2.56–2.53 Ga-late felsic volcanics in the Babina belt during 2542 ± 17 Ma. (4) 3.3Ga-the Bundelkhand Gneissic Complex (BnGC) of the Meso- Neoproterozoic age [12]. BuC also consists of different types of gneisses named after their mineral assemblages, such as garnet sillimanite gneisses, biotite sillimanite gneiss, garnet biotite amphibolites gneiss, amphibolites, calc-silicates, and granite gneisses. Two events of metamorphism and four major deformation phases are identified in the core region of BuC [13].

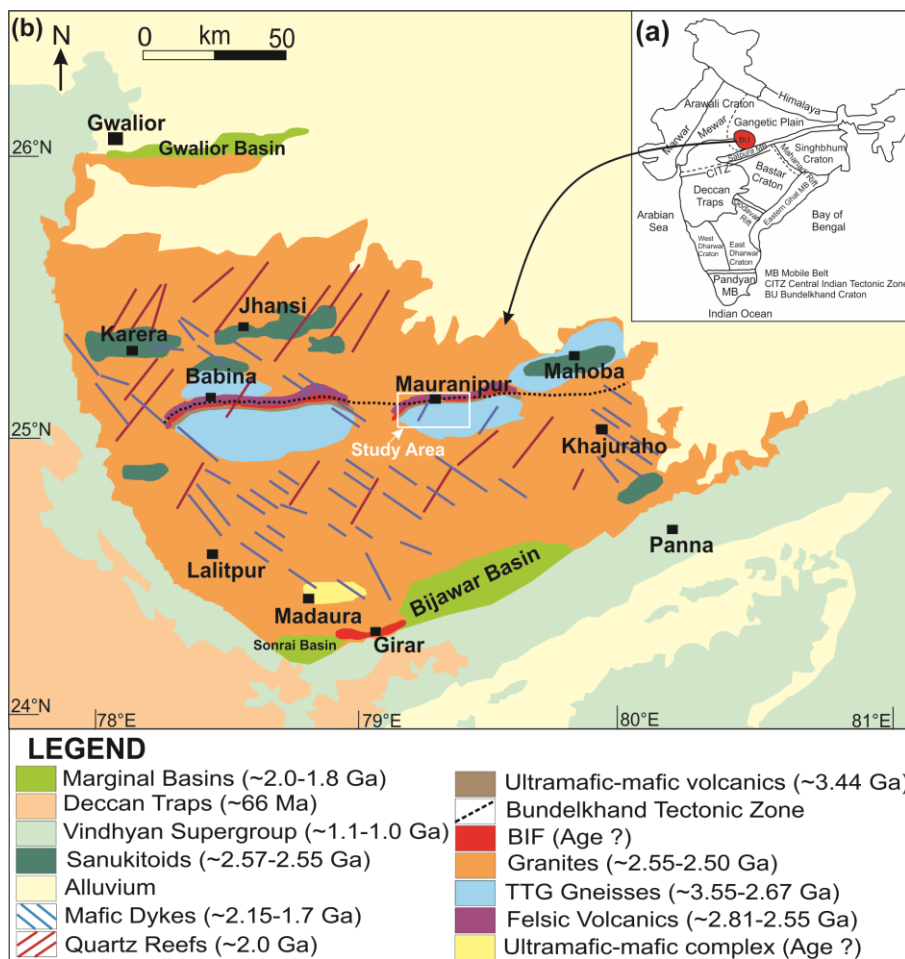


Figure 1. (a) Map of India showing the location of BuC. (b) Geological map of BuC [6]

The studied area is the Saprar river section near Kuraicha, Mauranipur, where unweathered rocks are exposed. Here, gneissic rocks are exposed in patches. There are also scattered ESE–WNW trending outcrops of banded magnetite quartzite and NE–SW trending quartz reefs. Multiphase deformation and folding are common. Deformation occurred in four events, D1–D4, in the area. The mesoscopic folds of the F1, F2, and F3 generations represent D1–D3 deformation, whereas the D4 deformation is characterized by rock shear structures [13].

Materials and methods

Sampling

Almost 30 samples of the garnet-bearing rocks were collected from the study area, from which five representative samples (K-2, K-3, K-4, K-5, K-6, and K-7) were chosen for the various analyses. In the field, these gneissic rocks are commonly associated with other igneous and metamorphic rocks. Gneissic rocks are dark-coloured in comparison to other rocks. Because of the prevalence of garnet, gneissic rocks are medium-to-coarse-grained, with a grey-to-pinkish tint and a greasy appearance. The collected samples are generally fresh. Garnet occurs as a significant constituent, having a pinkish hue. Light pink to white plagioclase crystals can be easily seen in hand specimens.

XRF Analysis

A whole rock analysis of representative samples for major oxides from the Mauranipur area, Jhansi, was done at the Birbal Sahni Institute of Palaeosciences (BSIP), Lucknow, India. Firstly, fresh rock samples were chipped with the help of a jaw crusher, and then an agate mortar was used for powdering the chips of the rock samples. All the work was done with precision to prevent contamination. In the pressed powder method, boric acid was used as the binder (sample ratio, 2:3) for preparing the sample. The XRF technique was used to analyze major oxides using a wavelength dispersive (WD-XRF AXIOS MAX) machine with 4KW, 60kV-160 mA analytical power on a pressed powder pellet machine using 'kameyo' at a pressure of 15-20 tonnes with a 4mm pallet thickness. All the data sets will be below 5% error with a good calibration curve.

Results

Geochemical characterization

The main, trace and REE data of the garnet-bearing rocks analyzed are presented in [Table 1](#), with ignition loss ranging from 0.27 to 0.54 for all samples. The gneissic rocks are compositionally variable in major oxides such as SiO₂ (62.25–66.32 wt%), Al₂O₃ (17.58–19.09 wt%), MgO (1.50–3.40 wt%), FeO (7.10–8.01 wt%), K₂O (1.86–2.68 wt%), and also contain lesser amounts of TiO₂ (0.61–0.72 wt%), CaO (1.33–2.75 wt%), Na₂O (1.26–2.36 wt%), and P₂O₅ (0.07–0.27 wt%). From the Harker variation diagrams ([Fig. 2](#)), it has been deduced that the MgO, CaO, MnO, Na₂O, and K₂O continuously decrease with increasing SiO₂, whereas the Al₂O₃, FeO, and TiO₂ increase with increasing SiO₂. The total alkali vs silica [14] diagram ([Fig. 3a](#)) illustrates that the gneissic rocks are diorite and granodioritic in nature, implying that the gneissic rocks were derived from different sedimentary environments. Moreover, the (SiO₂) versus (Na₂O+K₂O-CaO) plot shows calcic to calc-alkalic composition ([Fig. 3b](#)). Most of the samples are ferroan, with two samples of gneissic rocks

showing magnesian character (Fig. 3c). However, the SiO₂ versus K₂O diagram (Fig. 3d) illustrates that the medium K calc-alkaline series dominates gneissic rocks. The A/NK vs A/CNK diagram (Fig. 3e) shows that all samples are peraluminous (A/CNK = 2.48–4.28). The Na₂O versus K₂O diagram (Fig. 3f) represents shoshonitic and ultra-potassic composition. The variation of the different major oxides with SiO₂ illustrates a substantial role in the fractionation and crystallization of minerals during the successive evolution of parental magma. The fractionation of feldspar can be depicted by the fall of Al₂O₃ with increasing SiO₂. The variation diagrams of trace elements such as Ba and Sr have been effectively used to evaluate fractional crystallization processes [15]. In this study, Ba and Sr decrease with increasing SiO₂, suggesting an early fractionation of plagioclase and K-feldspar in gneissic rocks. This is supported by the presence of negative Eu and Sr anomalies.

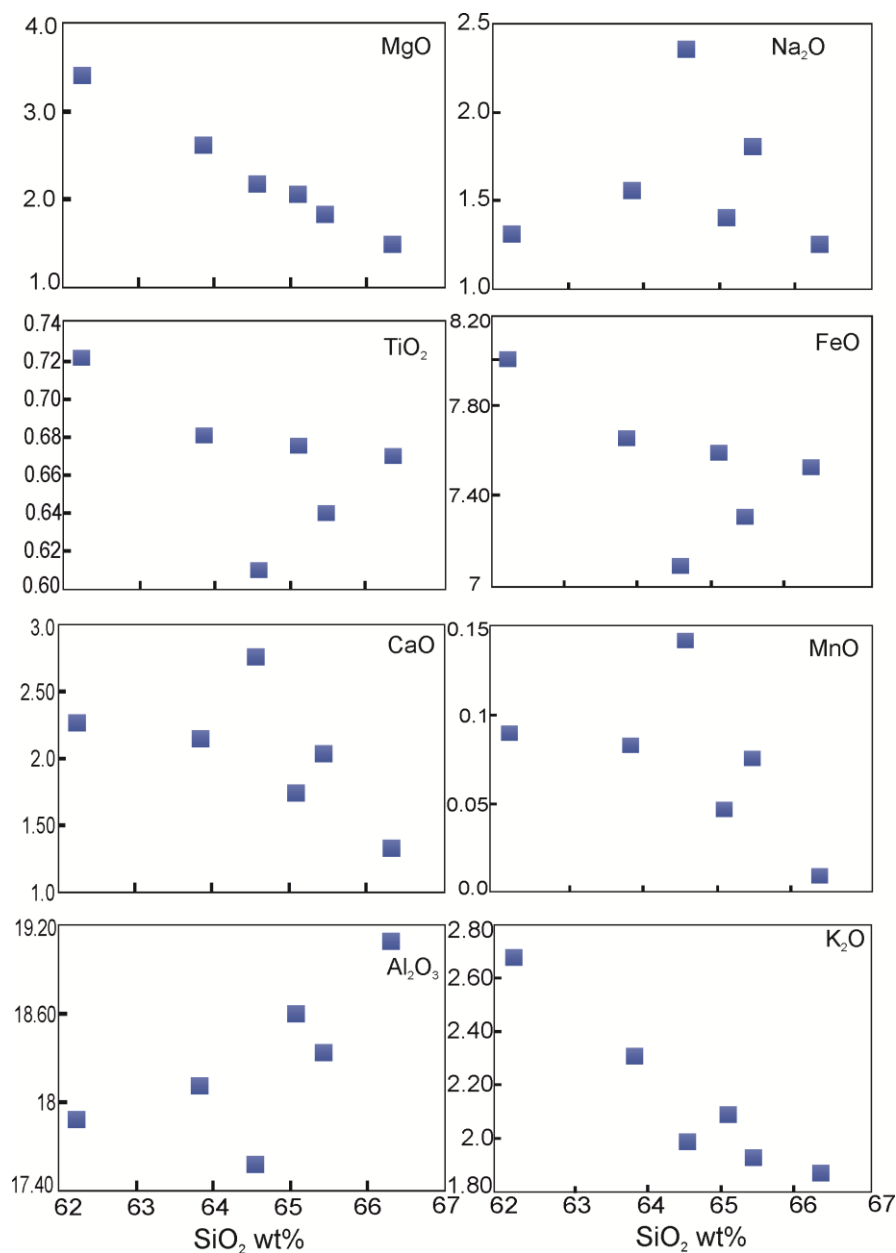


Figure 2. Harker Variation plot of major oxides vs SiO₂.

Table 1. Representative major oxides (in wt%), trace elements and REEs (in ppm) compositions of gneissic rocks.

Major oxides	K-2	K-3	K-4	K-5	K-6	K-7
SiO ₂	66.32	64.56	65.44	62.25	63.85	65.08
Al ₂ O ₃	19.09	17.58	18.34	17.89	18.11	18.60
TiO ₂	0.67	0.61	0.64	0.72	0.68	0.67
FeO	7.53	7.10	7.32	8.01	7.66	7.60
MnO	0.01	0.14	0.08	0.09	0.08	0.05
MgO	1.50	2.18	1.84	3.4	2.62	2.06
CaO	1.33	2.75	2.04	2.26	2.15	1.74
Na ₂ O	1.26	2.36	1.81	1.32	1.57	1.41
K ₂ O	1.86	1.99	1.93	2.68	2.30	2.08
P ₂ O ₅	0.08	0.27	0.17	0.07	0.12	0.10
LOI	0.27	0.42	0.34	0.54	0.44	0.35
TOTAL	99.93	99.95	99.94	99.23	99.59	99.76
V	72.06	56.89	64.48	60.68	68.27	58.79
Co	19.28	17.06	18.17	17.62	18.73	17.34
Ni	33.8	28	30.90	29.45	32.35	28.73
Cu	102.8	175	138.90	156.95	120.85	165.98
Zn	96.8	112.2	104.50	108.35	100.65	110.28
Rb	125.1	141.8	133.45	137.63	129.28	139.71
Sr	16	25	20.50	22.75	18.25	23.88
Zr	201	165.6	183.30	174.45	192.15	170.03
Nb	7.3	9.7	8.50	9.10	7.90	9.40
Mo	2.69	3.64	3.17	3.40	2.93	3.52
Cd	0.12	0.24	0.18	0.21	0.15	0.23
Ba	569	459	514.00	486.50	541.50	472.75
Hf	3.62	2.64	3.13	2.89	3.38	2.76
Ta	0.25	0.3	0.28	0.29	0.26	0.29
Pb	8.5	17.2	12.85	15.03	10.68	16.11
Th	28.1	21.59	24.85	23.22	26.47	22.40
U	2.6	2.78	2.69	2.74	2.65	2.76
La	90.17	73.57	81.87	86.02	83.95	77.72
Ce	198	119	158.5	178.25	168.38	138.75
Pr	22	19.2	20.6	21.30	20.95	19.90
Nd	81	64.5	72.75	76.88	74.81	68.63
Sm	14.6	9.4	12	13.30	12.65	10.70
Eu	1.92	1.41	1.665	1.79	1.73	1.54
Gd	13.98	8.82	11.4	12.69	12.05	10.11
Tb	1.65	1.09	1.37	1.51	1.44	1.23
Dy	7.21	4.63	5.92	6.57	6.24	5.28
Ho	1.12	1.54	1.33	1.23	1.28	1.44
Er	2.42	1.64	2.03	2.23	2.13	1.84
Tm	0.25	0.19	0.22	0.24	0.23	0.21
Yb	1.31	1.75	1.53	1.42	1.48	1.64
Lu	0.17	0.38	0.275	0.22	0.25	0.33
Y	30.08	21.78	25.93	28.01	26.97	23.86
(La/Sm) _N	3.99	5.05	4.40	4.18	4.28	4.69
(La/Lu) _N	56.85	20.75	31.91	41.43	36.17	25.43
Eu/Eu*	0.41	0.47	0.44	0.42	0.43	0.45

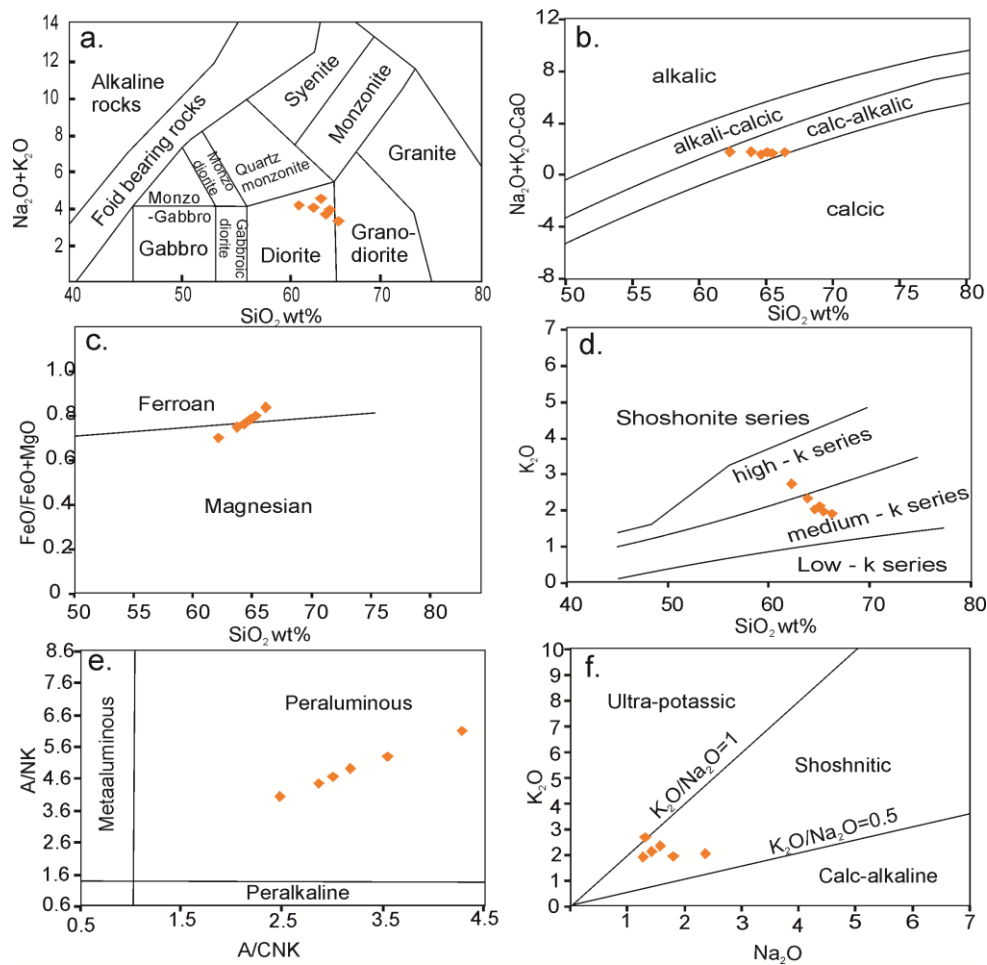


Figure 3. Chemical classification diagrams using major element composition of the studied rocks. (a) Total alkali versus silica (TAS) diagram for plutonic rocks after [14], (b) Calcic to alkali-calcic via calc-alkaline nature of studied rocks. (c) Granitoid classification scheme [26] revealing magnesian to ferroan. (d) K_2O versus SiO_2 plot after [27]. (e) A/CNK versus A/NK diagram. (f) Na_2O versus K_2O diagram [28].

The trace and REEs element data of gneissic rocks show contrast values of incompatible elements such as Rb (125.1–141.8 ppm), Sr (16–25 ppm), Ba (486.50–569 ppm), Y (21.78–30.08 ppm), Th (21.59–28.1 ppm) and U (2.6–2.78 ppm) as well as compatible elements such as Ni (28–33.8 ppm), and Co (17.06–19.28 ppm) (Table 1). Multi-element diagrams normalized on the primitive mantle reveal distinctive depletion of Mo, Ho, Tm, Nb, Ta, Sr, Hf, Ti, and an abundance of Rb, Ba, La, Ce, and Gd (Fig. 4a). The wide range of high field-strength elements (HFSEs) may be due to the degrees of mobility of the elements during the evolution of rock from the parental rock and under varying conditions of metamorphism. The presence of ilmenite can lead to the depletion of Ti. The chondrite normalized REE plot is depicted in Figure 4b. All the samples of gneissic rocks show a steady and nearly smooth REE pattern. The REE chondrite normalized patterns (Fig. 4b) show enriched LREE and depletion in HREE with negative Eu anomalies (0.41–0.47). The europium anomaly indicates the fractionation of the plagioclase during the evolution of magma. The LREE to HREE (La/Lu)_N ratio varies from 20.75–56.85. The chondrite normalized REEs pattern

has an enriched LREE relative to HREE and a negative Eu anomaly, which explains the parental rock's plagioclase-rich composition. The observed geochemical data and variation plots for the gneissic rocks support the idea of fractional crystallization during the evolution of their parental rock. Specific elemental ratios can assess the source rock and evolutionary trend characteristics [16]. The HFSEs such as Ti, Zr, Y, V, Cr, Ni, and REEs are the elements that remain immobile in comparison to the large ion lithophile elements (LILEs) such as K, Rb, Sr, and Ba, as well as Th and U during metamorphism and erosion. Therefore, they are suitable for determining the parental rock's nature and chemical characteristics before metamorphism [17]. The high Rb/Sr and Ba/Sr ratios and relative enrichment of HFSE suggest that a source of felsic nature is the protolith of gneissic rocks.

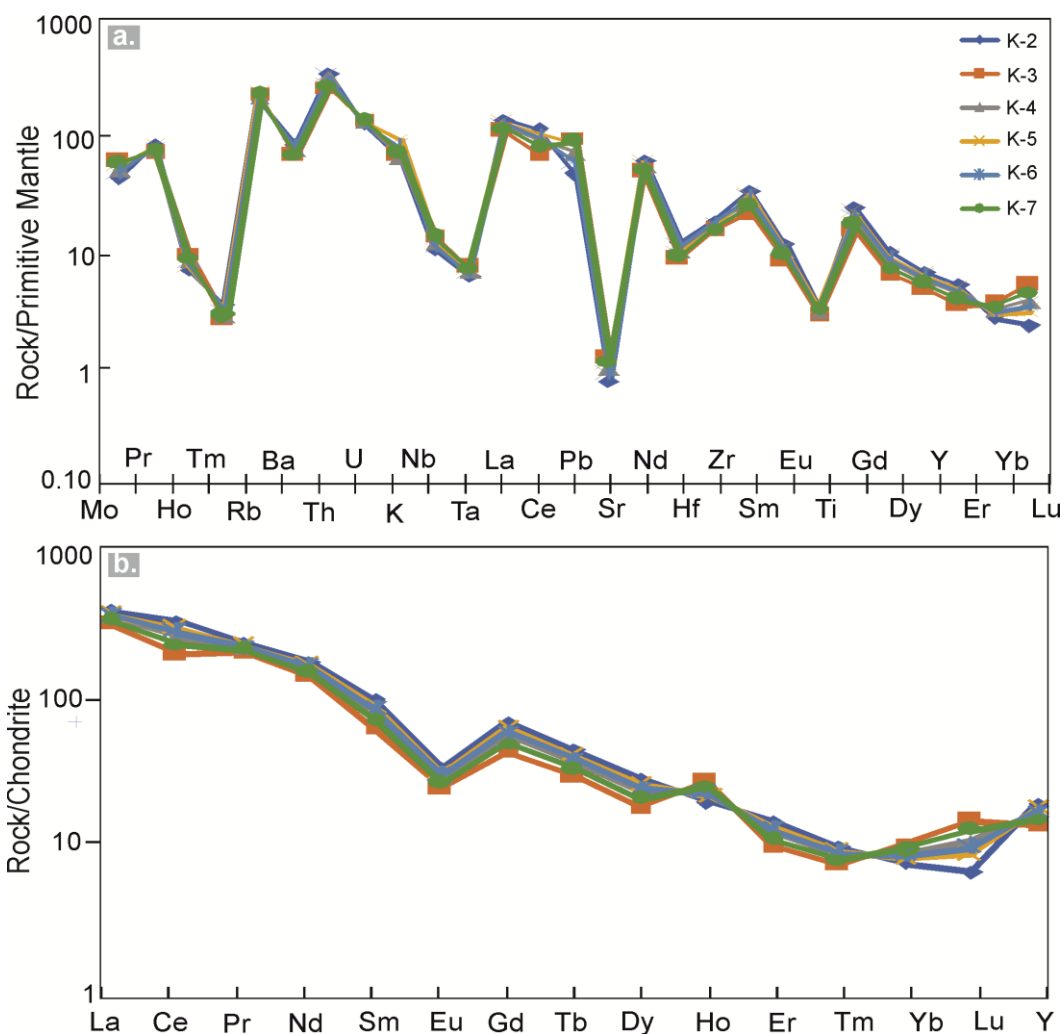


Figure 4. (a) Primitive mantle normalized multi-element spider diagram of aluminium silicate rocks. Normalized values are after [29]. (b) Chondrite normalized rare earth element plot. Normalized values are after [29].

The Nature of the Original Sediments

Sample data plots have been shown on the discrimination diagram (Fig.5a) of $\log(\text{Fe}_2\text{O}_3/\text{K}_2\text{O})$ vs $\log(\text{SiO}_2/\text{Al}_2\text{O}_3)$ [18] to characterize the lithological characteristics of the original

sediment. It represents a distinct set of data plots in the shale field, whereas one sample lies on the line between shale and Fe-shale fields. The P_2O_5/TiO_2 vs MgO/CaO [19] plot indicates the recycled sedimentary origin of the rocks (Fig.5b). However, there are no decisive criteria to recognize the characteristics of the primitive magmatic material of the reworked sediments. However, [20] has developed some discrimination plots. Elements have minimal mobility during sedimentary processes and are used to distinguish between different igneous source rocks. The Chemical Index of Alteration (CIA) vs. Index of Compositional Variability (ICV) discrimination diagram also shows the recycled metasediments as the protolith of the gneissic rocks themselves, which originated from an andesitic source (Fig.5c) [21]. The data point cluster on the SiO_2 vs $\log(K_2O/Na_2O)$ diagram [22] for the protolith of gneissic rocks suggests that the depositional environment was an active continental margin (ACM) (Fig.5d).

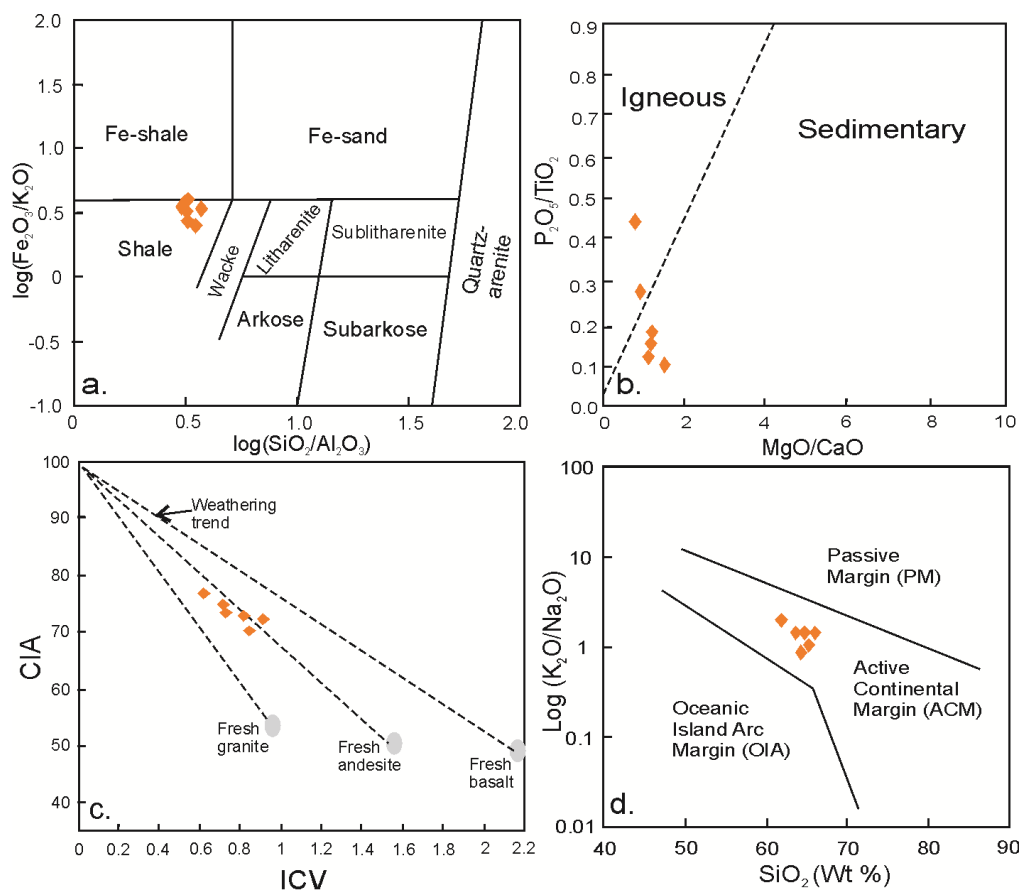


Figure 5. (a) $\log(SiO_2/Al_2O_3)$ vs $\log(Fe_2O_3/K_2O)$ plot after [18], (b) The MgO/CaO vs P_2O_5/TiO_2 diagram after [19], (c) CIA versus ICV diagram of [21], (d) SiO_2 vs. $\log(K_2O/Na_2O)$ diagram after [22].

Provenance and tectonic setting

The provenance of the gneissic rocks is established with the help of discrimination function analysis, in which the major oxides and trace elements have been utilized [22]. This discrimination function analysis differentiates four provenance fields: mafic igneous, intermediate igneous, felsic igneous, and quartzose sedimentary or recycled provenance. When plotted in the

discrimination function diagram (Fig. 6a), the gneissic rocks acquire the domain of felsic igneous provenance. The TiO_2 versus Zr plot confirms this, as all the gneissic rocks are again plotted in the felsic igneous rock field (Fig. 6b). The trace-element data are used to generate tectonic discrimination diagrams that highlight the parental rock's characteristics and the type of tectonism. The $(Th/Nb)_N$ vs $(Y/Nb)_N$ ratio indicates that the gneissic rocks form in a convergent tectonic setting (Fig. 6c). The Nb/Zr vs Zr plot shows that the studied rocks are formed by the subduction process (Fig. 6d). The Y vs Nb plot suggests that the protolith of the gneissic rocks was derived from volcanic arc granite (VAG) and a syn-collisional tectonic environment (Fig. 6e), whereas the Y+Nb vs Rb plot clarifies that the protolith was derived from VAG (Fig. 6f).

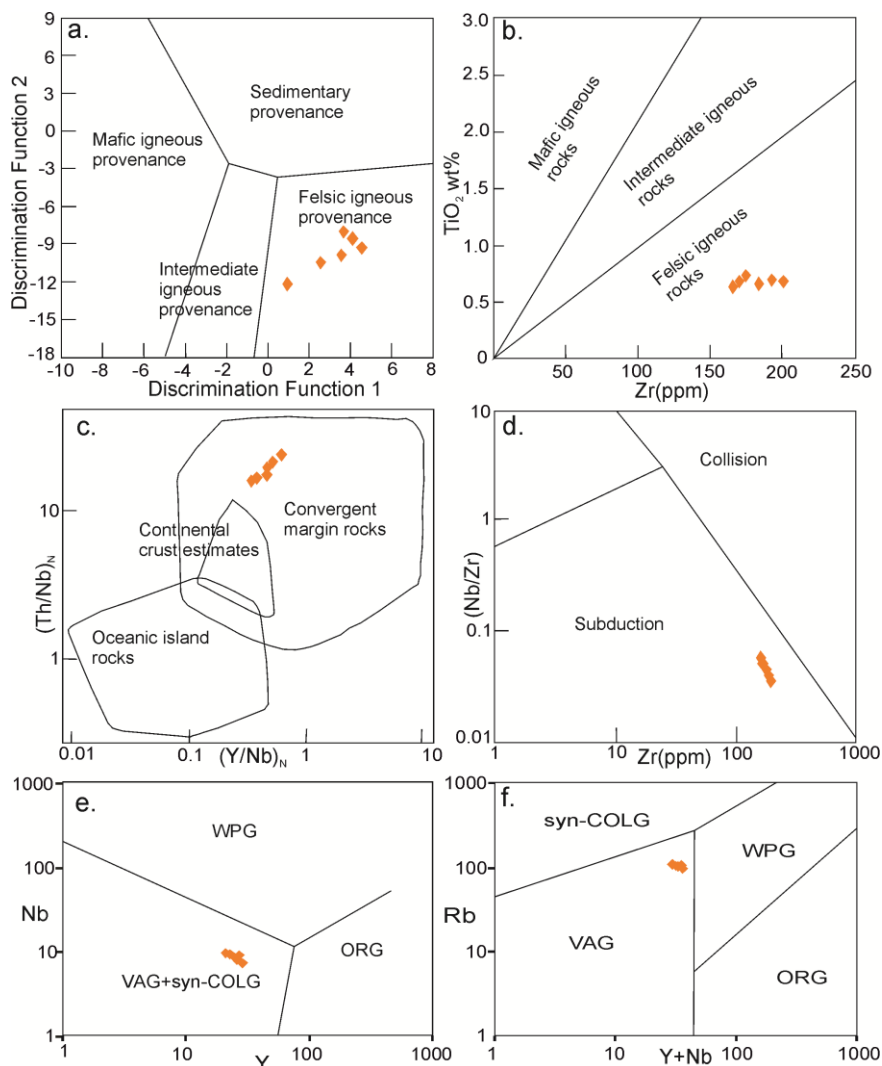


Figure 6. (a) Major element Discriminant Function diagram for provenance [30] where Discriminant Function 1 = $(-1.773 TiO_2) + (0.607 Al_2O_3) + (0.760 Fe_2O_3) + (-1.500 MgO) + (0.616 CaO) + (0.509 Na_2O) + (-1.224 K_2O) + (-9.090)$; Discriminant Function 2 = $(0.445 TiO_2) + (0.070 Al_2O_3) + (-0.250 Fe_2O_3) + (-1.142 MgO) + (0.438 CaO) + (1.475 Na_2O) + (-1.426 K_2O) + (-6.861)$. (b) TiO_2 –Zr plot [31] (c) $(Y/Nb)_N$ versus $(Th/Nb)_N$ diagram [32], (d) Zr versus Nb/Zr plot [33] (e) Y vs Nb tectonic discrimination diagram. (f) Y+Nb vs Rb tectonic discrimination plot. Syn-COLG: syn-collisional granite; WPG: within plate granite; VAG: volcanic arc granite; ORG: ocean ridge granite [34].

Discussion and conclusions

Based on the normalized trace and rare-earth element (REE) patterns and discrimination diagrams, we have concluded the nature of the parental rock and tectonic settings of the studied gneissic rocks during their formation. Geochemical attributes added with field observations and discrimination diagrams appear to be helpful for the characterization of gneissic rocks. According to the geochemical study, the gneissic rocks are formed by the deposition of felsic sediments in a convergent margin and are then metamorphosed. The time since sedimentation and their source locality with the metamorphism after the deposition play a vital role in uncovering the tectonic history. Gneissic rocks are formed by the accumulation and diagenesis of weathering products from pre-existing rocks. However, these rocks are continuously exposed to erosion, leading to severe discordant patterns in the BuC. The present study concludes:

- The gneissic rocks of the study area have preserved various deformation structures, indicating that they experienced multiple phases of deformation events.
- Based on Harker variation diagrams, gneissic rocks evolved from the magma separation process (Fig. 2).
- These rocks were plotted on the TAS plot (Fig.3a), showing the provenance is of the dioritic composition. The granodioritic magma has concentrated plagioclase during fractional crystallization, and its ascent must have given rise to the parental rock of the gneissic rocks.
- Gneissic rocks are enriched in K, Th, Rb, Zr, Sm, and Y and depleted in Ba, Nb, Ta, and Ti. A negative anomaly of Nb and Ti suggests a subduction-related environment. Mixing of magma with the Earth's crust can explain the high concentration of Rb. LREE to HREE are in moderate concentration in the samples, and a negative anomaly of Eu is also considerable ($\text{Eu}/\text{Eu}^* = 0.41-0.47$). Usually, feldspars are responsible for Eu anomalies since Eu in its bivalent state is compatible with calcium feldspars, while the rest of the trivalent REEs are not. As a result, when calcium feldspar is separated from the parental rock, Eu leads to a negative anomaly.
- The $\log(\text{Fe}_2\text{O}_3/\text{K}_2\text{O})$ vs $\log(\text{SiO}_2/\text{Al}_2\text{O}_3)$ plot (Fig.5a) demarcates that the sediments were derived from the dioritic arc to form shale after the deposition in the sedimentary basin. Furthermore, another discrimination diagram, CIA vs ICV, depicts the recycled metasediments, where the protolith is generated from the granitic source (Fig.5c). The tectonic discrimination diagram suggested the protolith of gneissic rocks were deposited in the ACM (Fig.5d). The ICV range is 0.79 to 1.08, suggesting gneissic rocks were initially formed as immature sediments and are likely to have been deposited in ACM tectonic settings. Silicification and K-metasomatism are significant processes that play an important role in modifying post-depositional sediments [23–25]. Subsequently, significant changes were observed. Major elements like; Fe, Mg, Ca, and Na leached out of the sediments, whereas Si and K concentrated [23].
- The parental rock of gneissic rocks was derived from felsic igneous provenance (Fig. 6a&b) within a convergent margin tectonic setting (Fig. 6c&d). Although, the various geochemical ratios (e.g., Y/Nb, Y+Nb/Rb) demonstrate that the parental rock of gneissic rocks was derived from the volcanic arc granite and syn-collisional setting (Fig. 6e&f).

This study proposes that the Bundelkhand gneissic rocks are derived mainly from a granitic source in a subduction zone. However, detailed research to determine this tectonic evolution would require more geochemical and geochronological data on various rock types.

Acknowledgements

We thank the Director, IIT (BHU), for providing the infrastructure to carry out our work. Pratigya Pathak is grateful to the MHRD Fellowship Scheme for providing financial support.

References

- [1]. H.Y. Madukwe, O.A.I Bigbami and R.A.O. Basi, "Assessment of Trace and Rare Earth Element Levels in Stream Sediments in Ijero-Ekiti Area, Southwest Nigeria," *Nature Env. Pollution Tech.*, vol. 19, no. 2, pp. 421–439, 2020.
- [2]. B. Castor and B.H. James, "Rare earth elements," in E.K. Jessica, CT Nikhil, MB James (eds.), *Industrial Minerals and Rocks*. Society for Mining, Metallurgy and Exploration, 2006, pp. 769–792.
- [3]. Z.H. Chen, "Global rare earth resources and scenarios of future rare earth industry," *J. Rare Earths*, vol. 29, pp. 1–6, 2018.
- [4]. E.P.A, "Rare Earth Elements: A Review of Production, Processing, Recycling, and Associated Environmental Issues," EPA600/R-12/572, 2012.
- [5]. S.G. Gokarn, C.K. Rao, C. Selvaraj, G. Gupta and B.P. Singh, "Crustal Evolution and Tectonics of the Archean Bundelkhand Craton, Central India," *J. Geol. Soc. India*, vol. 82, pp. 455–460, 2013.
- [6]. P.K. Singh, S.K.Verma, V.K.Singh, J.A. Moreno, V.P. Malviya, E.P. Oliveira, X.H. Li, V.P. Malviya and D. Prakash. Geochronology and petrogenesis of the TTG gneisses and granitoids from the Central Bundelkhand granite-greenstone terrane, Bundelkhand Craton, India: Implications for Archean crustal evolution and cratonization. *Precamb. Res.* 2021; 359, 106–210.
- [7]. P.K. Singh, S.K. Verma, J.A. Moreno, V.K. Singh, V.P. Malviya, E.P. Oliveira, S. Mishra and M. Arima. Geochemistry and Sm-Nd isotope systematics of mafic-ultramafic rocks from the Babina and Mauranipur greenstone belts, Bundelkhand Craton, India: Implications for tectonic setting and Paleoproterozoic mantle evolution. *Lithos.* 2019; 330–331, 90–107.
- [8]. A.K. Basu. Some characteristics of the Precambrian crust in the northern part of Central India. *Geol. Sur. India special publication.* 2001; 55, 181–204.
- [9]. S.P. Singh and S.B. Dwivedi. High-grade metamorphism of the Bundelkhand massif and its implications for crustal evolution of the middle archean crust of central India. *J. Earth Sys. Sci.* 2015; 124, 197–211.
- [10]. A. Slabunov and V. Singh. Meso-Neoproterozoic crustal evolution of the Bundelkhand Craton, Indian Shield: new data from greenstone belts. *Int. geol. Review.* 2019; 61, 1409–1428.
- [11]. V. Singh and S. kumar. Geochemistry of granitic rocks of Bundelkhand Craton and its origin, International conference on recent advances in material and chemical sciences, geology review. 2017.
- [12]. V.P. Malviya, M. Arima, J.K. Pati and Y. Kaneko. Petrology and geochemistry of metamorphosed basaltic pillow lava and basaltic komatiite in the Mauranipur area: Subduction related volcanism in the Archean Bundelkhand Craton, Central India. *J. Mineral. Petrol. Sci.* 2006; 101, 199–217.
- [13]. S.P. Singh and S.B. Dwivedi. Garnet sillimanite–cordierite–quartz bearing assemblages from the early Archean supracrustal rocks of Bundelkhand massif central India. *Curr. Sci.* 2009; 97, 103–107.
- [14]. E.A. Middlemost. Naming materials in the magma/igneous rock system. *Earth-Sci. Reviews.* 1994; 37(3–4), 215–224.
- [15]. J. Ray, A. Saha and S. Ganguly. Geochemistry and petrogenesis of Neoproterozoic Mylonitic granitoids, Meghalaya Plateau, northeastern India. *J. Earth Syst. Sci.* 2011; 120, 459.
- [16]. J.B. Whalen, K.L. Currie and B.W. Chappell. A-type granites: geochemical characteristics, discrimination and petrogenesis. *Contrib. Mineral. Petrol.* 1987; 95, 407–419.

- [17]. N.O. Setiawan, N. Yasuhito, A. Nobuhiko, Y. Tatsuro, Y. Kazuhiro, M. Aya, W. Kaharuddin and S.L. Joko. Geochemical characteristics of metamorphic rocks from South Sulawesi, Central Java, South and West Kalimantan in Indonesia; ASEAN Eng. J. Part C. 2014; 3, 107–127.
- [18]. M.M. Herron. Geochemical classification of terrigenous sands and shales from core or log data. *J. Sediment. Petrol.* 1988; 58, 820–829.
- [19]. C.D. Werner. Saxoniangranulites-igneous or lithoigneous: a contribution to the geochemical diagnosis of the original rock in high metamorphic complexes. *ZfS-Mitteilungen.* 1987; 133, 221–250.
- [20]. L. Pinto, G. Herail, B. Moine, F. Fonton, R. Charrier and B. Dupre. Using geochemistry to establish the igneous provenances of the Neogene continental sedimentary rocks in the Central Depression and Altiplano, Central Andes. *Sediment. Geol.* 2004; 166, 157–183.
- [21]. P.E. Potter, J.B. Maynard and P.J. Depetris. *Mud and Mudstones: Introduction and Overview*: Heidelberg, Springer-Verlag, 2005; 297 pp.
- [22]. B.P. Roser and R.J. Korsch. Provenance signatures of sandstone-mudstone suites determined using discriminant function analysis of major-element data. *Chem. Geol.* 1988; 67, 119–139.
- [23]. R.L. Cullers, M.J. Di Marco, D.R. Lowe and J. Stone. Geochemistry of a silicified, felsic volcanoclastic suite from the early Archaean Panorama Formation, Pilbara Block, Western Australia: an evaluation of depositional and post-depositional processes with special emphasis on the rare-earth elements. *Precamb. Res.* 1993; 60, 99–116.
- [24]. C.M. Fedo, H.W. Nesbitt and G.M. Young. Unraveling the effects of potassium metasomatism in sedimentary rocks and paleosoils, with implications for paleoweathering conditions and provenance. *Geol.* 1995; 23, 921–924.
- [25]. M.S. Tchouatcha, A.P. Kouske, A.S. Deaf and A.P. Mioumnde. Geochemical, mineralogical and sedimentological analyses of reworked sediments (new) in the syn- to post-rift Middle Cretaceous-Quaternary detrital deposits from western Atlantic margin of Cameroon: evidence from sedimentation-erosion alternation in the context of passive margin evolution. *ActaGeochim.* 2021; 40, 676–701.
- [26]. B.R. Frost, C.G. Barnes, W.J. Collins, R.J. Arculus, D.J. Ellis and C.D. Frost. A geochemical classification for granitic rocks. *J. Petrol.* 2001; 42(11), 2033–2048.
- [27]. A. Peccerillo and S.R. Taylor. Geochemistry of Eocene calc-alkaline volcanic rocks from the Kastamonu area, northern Turkey. *Contrib. Mineral. Petrol.* 1976; 58, 63–81.
- [28]. S. Turner, N. Amand, N. Rogers, C. Hawkesworth, N. Harris, S. Kelley, P. van Calsteren and W. Deng. Post-collision, shoshonitic volcanism on the Tibetan Plateau: Implications for convective thinning of the lithosphere and the source of ocean Island basalts. *J. Petrol.* 1996; 37, 45–71.
- [29]. S.S. Sun and W.F. McDonough. Chemical and isotopic systematic of oceanic basalts: Implications for mantle composition and processes. *Geol. Soc. London, Special Publication.* 1989; 42, 313–345.
- [30]. A.V. Murali, R. Parthasarathy, T.M. Mahadevan, and M.S. Das. Trace element characteristics, REE patterns and partition coefficients of zircons from different geological environments- A case study on Indian zircons. *Geochim. Cosmochim. Acta.* 1983; 47, 2047–2052.
- [31]. K. Hayashi, H. Fujisawa, H. Holland and H. Ohmoto. Geochemistry of ~1.9 Ga sedimentary rocks from northeastern Labrador, Canada. *Geochimica et Cosmochimica Acta.* (1997); 61(19), 4115–4137.
32. J.A. Moreno, J.F. Molina, P. Montero, M. Abu Anbar, J.H. Scarrow, A. Cambeses and F. Bea. Unraveling sources of A-type magmas in juvenile continental crust: Constraints from compositionally diverse Ediacaran post-collisional granitoids in the Katerina Ring Complex, southern Sinai, Egypt. *Lithos.* 2014; 56, 192–195.
- [32]. D. Thieblemont and M. Tegye. Geochemical discrimination of differentiated magmatic rocks attesting for the variable origin and tectonic setting of calc-alkaline magmas. *Comptes Rendus De Academie Des Sciences Series II.* 1994; 319, 87–94.
- [33]. J. Pearce, H. Nigel, and T. Andrew. Trace Element Discrimination Diagrams for the Tectonic Interpretation of Granitic Rocks. *J. Petrol.* 1984; 25.